Available online at www.sciencedirect.com
SCIENCE DIRECT®
Thermochimica Acta 406 (2003) 35–53
thermochimica acta
www.elsevier.com/locate/tca

Plasma power source based on a catalytic reaction of atomic hydrogen measured by water bath calorimetry

R.L. Mills*, X. Chen, P. Ray, J. He, B. Dhandapani

BlackLight Power Inc., 493 Old Trenton Road, Cranbury, NJ 08512, USA

Received 27 June 2002; received in revised form 17 December 2002; accepted 3 April 2003

Abstract

Extreme ultraviolet (EUV) spectroscopy was recorded on microwave discharges of helium with 2% hydrogen. Novel emission lines were observed with energies of $q \times 13.6$ eV, where $q = 1, 2, 3, 4, 6, 7, 8, 9, 11$ or these discrete energies less 21.2 eV corresponding to inelastic scattering of these photons by helium atoms due to excitation of He ($1s^2$) to He ($1s^1 2p^1$). The average hydrogen atom temperature was measured to be 180–210 eV versus ≈3 eV for pure hydrogen. The electron temperature T_e for helium–hydrogen was 30,500 ± 5% K compared to 7400 ± 5% K for pure helium. Dominant He^+ emission and an intensification of the plasma emission observed when He^+ was present with atomic hydrogen demonstrated the role of He^+ as a catalyst. Using water bath calorimetry, excess power was observed from the helium–hydrogen plasma compared to control krypton plasma. For example, for an input of 8.1 W, the total plasma power of the helium–hydrogen plasma measured by water bath calorimetry was 30.0 W corresponding to 21.9 W of excess power in 3 cm^3. The excess power density and energy balance were high, 7.3 W/cm^3 and -2.9×10^4 kJ/mole H_2, respectively.

Keywords: Extreme ultraviolet spectroscopy; Helium–hydrogen plasma; Doppler broadening

1. Introduction

A new chemically generated or assisted plasma source has been developed that is based on a resonant energy transfer mechanism (rt-plasma). One such source operates by incandescently heating a hydrogen dissociator and a catalyst to provide atomic hydrogen and gaseous catalyst, respectively, such that the catalyst reacts with the atomic hydrogen to produce a plasma. It was extraordinary that intense extreme ultraviolet (EUV) emission was observed by Mills et al. [1–3] at low temperatures (e.g. ≈10^3 K) and an extraordinary low field strength of about 1–2 V/cm from atomic hydrogen and certain atomized elements or certain gaseous ions which singly or multiply ionize at integer multiples of the potential energy of atomic hydrogen, 27.2 eV. A number of independent experimental observations confirm that the rt-plasma is due to a novel reaction of atomic hydrogen which produces as chemical intermediates, hydrogen in fractional quantum states that are at lower energies than the traditional "ground" ($n = 1$) state. Power is released, and the final reaction products are novel hydride compounds. The supporting data include EUV spectroscopy [1–13,15,16,18,19], characteristic emission from catalysts and the hydride ion products [3,7,11,12], lower-energy hydrogen emission [4–10,18], chemically formed plasmas [1–3,11,12,15,16], Balmer

* Corresponding author. Tel.: +1-609-490-1090; fax: +1-609-490-1066.
E-mail address: rmills@blacklightpower.com (R.L. Mills).

0040-6031/$ – see front matter © 2003 Elsevier Science B.V. All rights reserved.
doi:10.1016/S0040-6031(03)00228-4

α line broadening [2–5,7,12–14,18,19], population inversion of H lines [18,19], elevated electron temperature [4,7,13,14], anomalous plasma afterglow duration [15,16], power generation [5–8,10,13,17,18], and analysis of novel chemical compounds [20,21].

The theory given previously [22–24] is based on applying Maxwell's equations to the Schrödinger equation. The familiar Rydberg equation (Eq. (1)) arises for the hydrogen excited states for $n > 1$ of Eq. (2).

$$E_n = -\frac{e^2}{n^2 8\pi\varepsilon_0 a_H} = -\frac{13.598\,\text{eV}}{n^2} \quad (1)$$

$$n = 1, 2, 3, \ldots \quad (2)$$

An additional result is that atomic hydrogen may undergo a catalytic reaction with certain atoms and ions which singly or multiply ionize at integer multiples of the potential energy of atomic hydrogen, $m \times 27.2\,\text{eV}$, wherein m is an integer. The reaction involves a nonradiative energy transfer to form a hydrogen atom that is lower in energy than unreacted atomic hydrogen that corresponds to a fractional principal quantum number. That is

$$n = \frac{1}{2}, \frac{1}{3}, \frac{1}{4}, \ldots, \frac{1}{p}; \quad p \text{ is an integer} \leq 137 \quad (3)$$

replaces the well known parameter $n =$ integer in the Rydberg equation for hydrogen excited states. The $n = 1$ state of hydrogen and the $n = 1/\text{integer}$ states of hydrogen are nonradiative, but a transition between two nonradiative states, say $n = 1$ to 1/2, is possible via a nonradiative energy transfer. Thus, a catalyst provides a net positive enthalpy of reaction of $m \times 27.2\,\text{eV}$ (i.e. it resonantly accepts the nonradiative energy transfer from hydrogen atoms and releases the energy to the surroundings to affect electronic transitions to fractional quantum energy levels). As a consequence of the nonradiative energy transfer, the hydrogen atom becomes unstable and emits further energy until it achieves a lower-energy nonradiative state having a principal energy level given by Eqs. (1) and (3). Processes such as hydrogen molecular bond formation that occur without photons and that require collisions are common [25]. Also, some commercial phosphors are based on resonant nonradiative energy transfer involving multipole coupling [26].

We propose that atomic hydrogen may undergo a catalytic reaction with He^+ which ionizes at two times the potential energy of atomic hydrogen, $2 \times 27.2\,\text{eV}$. Thus, microwave discharges of helium–hydrogen mixtures were studied by EUV spectroscopy to search for line emission from transitions to fractional Rydberg states of atomic hydrogen. Since the electronic transitions are very energetic, Balmer α line broadening, electron temperature, and power balances were measured to determine whether this reaction has sufficient kinetics to merit its consideration as a practical power source.

2. Experimental

EUV spectroscopy was recorded on hydrogen, xenon, helium, xenon–hydrogen (98/2%), and helium–hydrogen (98/2%) microwave discharge plasmas according to the methods given previously [6]. The experimental set up comprising a microwave discharge gas cell light source and an EUV spectrometer which was differentially pumped is shown in Fig. 1. A xenon–hydrogen (98/2%) or helium–hydrogen (98/2%) gas mixture was flowed at an inlet pressure of 1 or 20 Torr through a half inch diameter quartz tube fitted with a coaxial Evenson microwave cavity (Opthos), and each plasma of hydrogen, xenon, and helium alone was run at 20 Torr. The input power to the plasma from a microwave generator (Opthos model MPG-4M generator, frequency: 2450 MHz) was set at 85 W with forced air cooling of the cell. The spectrometer was a normal incidence 0.2 m monochromator (McPherson Model 302) equipped with a 1200 lines/mm holographic grating with a platinum coating that covered the region 2–560 nm. The EUV spectrum was recorded with a CEM. The wavelength resolution was about 0.2 nm (full-width at half-maximum (FWHM)) with slit widths of 50 μm. The increment was 0.2 nm and the dwell time was 500 ms. Peak assignments were based on a calibration against the known He I and He II lines.

The intensity of the hydrogen Lyman and Balmer emission was measured with the addition of 5% helium to a hydrogen glow discharge plasma. A diagram of a discharge cell light source and the experimental setup for discharge measurements is illustrated in Fig. 2. A hollow cathode and EUV spectrograph were aligned on a common optical axis using a laser. The vacuum ultraviolet emission spectrum was obtained

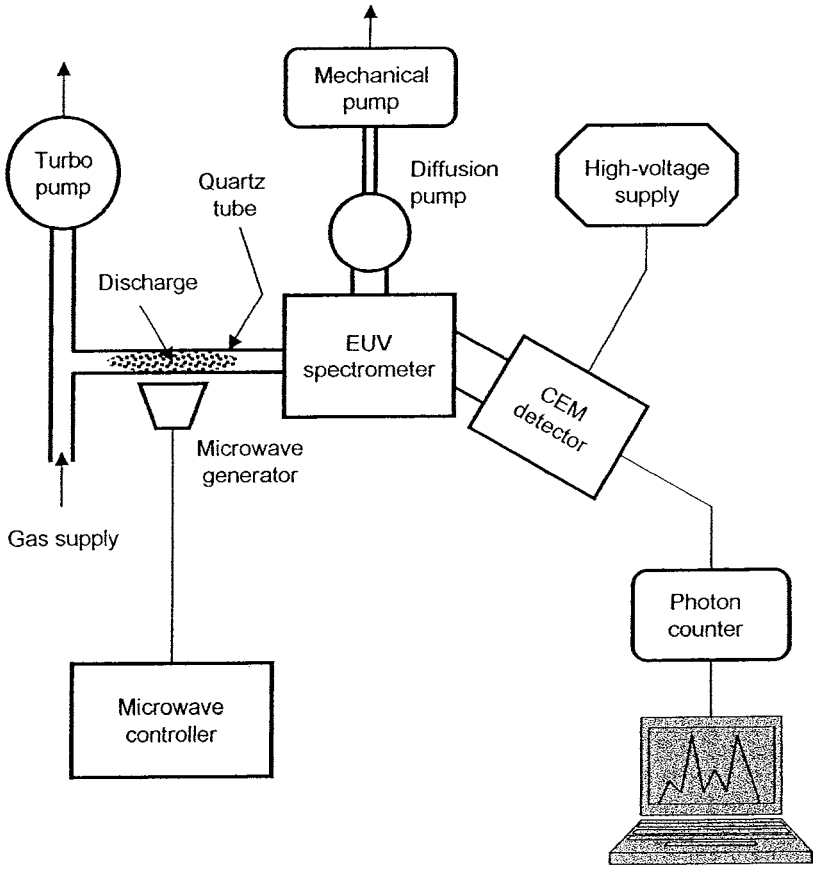

Fig. 1. The experimental set up comprising a microwave discharge gas cell light source and an EUV spectrometer which was differentially pumped.

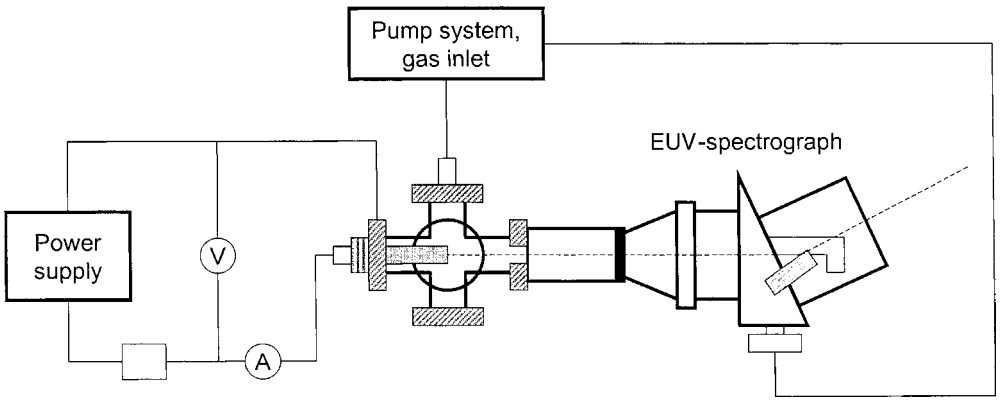

Fig. 2. The experimental set up of a discharge gas cell light source and a EUV spectrometer which was differentially pumped.

for hydrogen and helium–hydrogen (5/95%) plasma with a gas discharge cell that comprised a five-way stainless steel cross that served as the anode with a hollow stainless steel cathode. The plasma was generated at the hollow cathode (0.5 cm i.d.) inside the discharge cell. The hollow cathode was constructed of a stainless steel rod inserted into a steel tube, and this assembly was inserted into an Alumina tube. A flange opposite the end of the hollow cathode connected the spectrometer to the cell. It had a small hole that permitted radiation to pass to the spectrometer. An ac power supply (0–1 kV, 0–1 A) was connected to the hollow cathode to generate a discharge. The ac voltage and current at the time the EUV spectrum was recorded were 200 V and 40 mA, respectively. A Swagelok adapter at the very end of the steel cross provided a gas inlet and a connection with the pumping system, and the cell was pumped with a mechanical pump. Valves were located between the cell and the mechanical pump, the cell and the monochromator, and the monochromator and its turbo pump. The five-way cross was pressurized with 400 mTorr of gas which was maintained by flowing hydrogen or helium–hydrogen (5/95%) while monitoring the pressure with a 1 Torr absolute pressure gauge. The Lyman and Balmer emission were recorded with the normal incidence EUV spectrometer.

To achieve higher sensitivity at the shorter EUV wavelengths, the light emission from microwave plasmas of helium alone was recorded with a 4° grazing incidence EUV spectrometer equipped with a grating having 600 G/mm with a radius of curvature of ≈1 m that covered the region 5–65 nm. The monochromator angle of incidence was 87°. The resolution was about 0.4 nm (FWHM) with slit widths of 300 μm. A CEM was used to detect the EUV light. The increment was 0.1 nm and the dwell time was 1 s. In addition, the intensity of the emission of the He II peak at 30.4 nm was compared to that of the He I peak at 58.4 nm with the addition of 5% hydrogen to a helium microwave plasma at 1 Torr. The emission was recorded with the 4° grazing incidence EUV spectrometer.

The width of the 656.3 nm Balmer α line emitted from hydrogen alone, xenon–hydrogen mixture (90/10%), and helium–hydrogen mixture (90/10%) microwave discharge plasmas was measured with a high resolution visible spectrometer capable of a resolution of ±0.006 nm over the spectral range 190–860 nm [13,14]. The total pressure was 1 Torr, and the input power to the plasma was set at 40 W. The plasma emission was fiber-optically coupled through a 220 F matching fiber adapter positioned 2 cm from the cell wall to a Jobin Yvon Horiba 1250 M spectrometer with 2400 groves/mm ion-etched holographic diffraction grating. The entrance and exit slits were set to 20 μm. The spectrometer was scanned between 655.5 and 657.0 nm using a 0.005 nm step size. The signal was recorded by a photomultiplier tube (PMT) with a stand alone high voltage power supply (950 V) and an acquisition controller. The data was obtained in a single accumulation with a 1 s integration time. The electron density was determined using a Langmuir probe according to the method given previously [27].

To measure the absolute intensity, the high resolution visible spectrometer and detection system were calibrated [28] with 546.08, 576.96, and 696.54 nm light from a Hg–Ar lamp (Ocean Optics, model HG-1) that was calibrated with a NIST certified silicon photodiode. The population density of the $n = 3$ hydrogen excited state N_3 was determined from the absolute intensity of the Balmer α (656.28 nm) line measured using the calibrated spectrometer. The spectrometer response was determined to be approximately flat in the 400–700 nm region by ion etching and with a tungsten intensity calibrated lamp.

T_e was measured on microwave plasmas of helium alone and helium–hydrogen mixtures (90/10%) from the ratio of the intensity of the He 501.6 nm (upper quantum level $n = 3$) line to that of the He 492.2 nm ($n = 4$) line as described previously [14,29]. In each case, the total pressure was 0.1 Torr. The visible spectrum (300–560 nm) was recorded with the normal incidence EUV spectrometer with a photomultiplier tube and a sodium salicylate scintillator. The PMT (Model R1527P, Hamamatsu) used has a spectral response in the range of 185–680 nm with a peak efficiency at about 400 nm. The scan interval was 0.4 nm. The inlet and outlet slit were 300 μm with a corresponding wavelength resolution of 0.2 nm. The spectra were repeated five times per experiment and were found to be reproducible within less than 5%.

The excess power was measured by water bath calorimetry on helium–hydrogen (90/10%) plasmas compared to control plasmas with the same input power. The plasmas were maintained in a microwave discharge cell shown in Fig. 3. Each gas was ultrahigh pure. Each pure test gas was flowed through a half

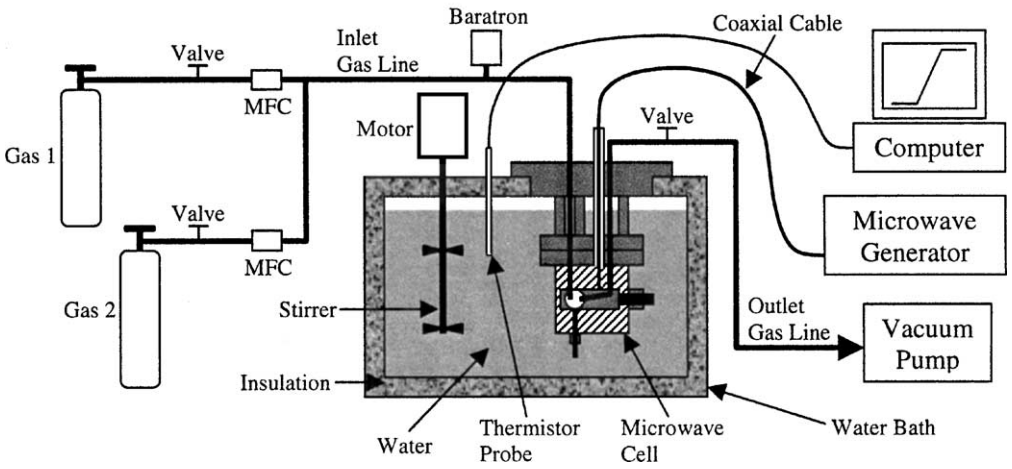

Fig. 3. Schematic of the water bath calorimeter. The Evenson cavity and a plasma-containing section of the quartz tube were fitted with a water-tight stainless steel housing, and the housing and cell assembly were suspended by four support rods from an acrylic plate which held the cell vertically from the top of a water bath calorimeter.

inch diameter quartz tube at 500 mTorr maintained with a noble gas or hydrogen flow rate of 10 sccm. After the calorimeter had reached a steady state, the pressure of the helium–hydrogen mixture was changed to 0.29 Torr. Each gas flow was controlled by a 0–20 sccm range mass flow controller (MKS 1179A21CS1BB) with a readout (MKS type 246). The cell pressure was monitored by a 0–10 Torr MKS Baratron absolute pressure gauge. The tube was fitted with an Evenson coaxial microwave cavity (Opthos) having an E-mode [30,31]. The microwave generator shown in Fig. 3 was an Opthos model MPG-4M generator (frequency: 2450 MHz).

The Evenson cavity and a plasma-containing section of the quartz tube were fitted with a water-tight stainless steel housing shown in Fig. 3. The housing comprised a 4 cm × 4 cm × 2 cm rectangular enclosure welded to a set of high vacuum 15.24 cm diameter conflat flanges. A silver plated copper gasket was placed between a mating flange and the cell flange. The two flanges were clamped together with 10 circumferential bolts. The top mating flange contained two penetrations comprising (1) a stainless steel thermocouple well (1 cm o.d.) housing a thermocouple probe in the cell interior that was in contact with the quartz tube wall adjacent to the Evenson cavity and (2) a centered 2.54 cm o.d. coaxial cable housing. The 1.27 cm o.d. quartz tube was sealed at its penetrations with the rectangular housing by Ultratorr fittings. The housing and cell assembly was suspended by four support rods from an 5.1 cm thick acrylic plate which held the cell vertically from the top of a water bath calorimeter shown in Fig. 3. The plate contained four sealed penetrations comprising (1) the stainless steel thermocouple well, (2) a 1 cm o.d. noble or hydrogen gas line, (3) a 1 cm o.d. vacuum line, and (4) the 2.54 cm o.d. coaxial cable housing. The gas inlet connected to a 0.64 cm o.d. flexible stainless steel tube that was connected by an Ultratorr seal to a welded-in 0.63 cm o.d. penetration of the rectangular enclosure. Inside of the enclosure, the penetration connected to the quartz tube by a 0.63–1.27 cm o.d. mating Ultratorr seal. The quartz tube had an elbow at the end opposite to the gas inlet penetration which attached to a 1 cm o.d. flexible stainless steel tube section of the vacuum line. The microwave cavity contained in the rectangular enclosure was tuned by a threaded tuning stub sealed in an end wall of the enclosure and a sliding tuning stub sealed with an Ultratorr fitting in the bottom wall. The sliding stub was tightened after the cell was tuned outside of the water bath, and the cell was immersed.

The water bath comprised an insulated reservoir filled with 45 L of distilled water. The water was agitated with a paddle driven by a stirring motor. A high

precision linear response thermistor probe (Omega OL-703) recorded the temperature of the water bath as a function of time for the stirrer alone to establish the baseline. The water bath was calibrated by a high precision heater (Watlow 125CA65A2X, with a Xantrex dc power supply 0–1200 ± 0.01 W). The heat capacity was determined for several input powers, 30, 40, and 50 W ± 0.01 W, and was found to be independent of input power over this power range within ±0.05%. The temperature rise of the reservoir as a function of time gave a slope in °C/s. This slope was baseline corrected for the negligible stirrer power and loss to ambient. The constant known input power (J/s), was divided by this slope to give the heat capacity in J/°C. Then, in general, the total power output from the cell to the reservoir was determined by multiplying the heat capacity by the rate of temperature rise (°C/s) to give J/s.

The power balance for a plasma system consisting of the contents of the water bath calorimeter is [17]

$$\dot{H} = \dot{M}(\hat{H}_{\text{in}} - \hat{H}_{\text{out}}) + \dot{Q}_{\text{plasma}} + \dot{Q}_{\text{power cable}} + \dot{Q}_{\text{stirrer}} + \dot{Q}_{\text{heat exchange}} \quad (4)$$

where H's are enthalpy values (inlet and outlet gases as indicated by the subscripts in and out, respectively, and the hat designates per mole), $\dot{M}$ the molar flow rate, and the $\dot{Q}$'s heat flow rates. It is clear from Eq. (4) that a correction must be considered both for the gas flow term (first term, right side), $\dot{Q}_{\text{power cable}}$ which represents the input of the short section (approximately 3 cm length) of the coaxial cable housing that passes through the water bath as it brings power to the microwave power coupler, for the work of the stirrer, and for the heat exchange between the insulated water bath and it surroundings.

The values of $\dot{Q}_{\text{power cable}}$ and the heat carried out with the gas were small, as determined by appropriate temperature readings. Thermocouples were employed to measure the temperature of the input and output gas, as well as the temperature of the coaxial cable housing just outside the water bath. Given that the temperature of the cable housing was never more than 3 K higher than the water bath $\dot{Q}_{\text{power cable}}$ can readily be shown to be negligible. The gas temperature change between input to the plasma and output from the water bath was never more than 1 K. Heat transfer from the quartz tube containing the flowing gas to the water in the bath was clearly very efficient. Given the maximum flow rate was 10 sccm, this requires a maximum correction of less than 10^{-5} W, a trivial correction. The stirrer and heat exchange terms were found to be the most significant correction, but its value was readily determined by measuring the temperature rise with only the stirrer operating. This correction can be accurately calculated from the slope of the pre- and post-heating periods and was found to be constant and of the order of 1 W for all experiments. Once these relatively trivial corrections are made the 'effective' energy balance becomes

$$\dot{H} = \dot{Q}_{\text{plasma}} \quad (5)$$

The calibration procedure resulted in a linear change in temperature for constant power inputs. This is expected given the nearly constant heat capacity of water over small changes in temperature (<3 K in all cases). Thus, changes in enthalpy can be readily equated with change in temperature of the bath. In short

$$\dot{H} = C_p \dot{T} = \dot{Q}_{\text{plasma}} \quad (6)$$

Thus, one must only multiply the calibration constant by the rate of change of bath temperature to obtain the plasma's heating power of the water bath. In the event that the change in temperature is nearly linear with time, as it was in all cases in this study, the rate (W) of heat input from the plasma to the bath can be readily determined, and compared with the microwave input power.

Quantifying the microwave input power to the plasmas was achieved by maintaining forward and reflected powers, as measured with power diodes, identical in all cases. That is, for both helium–hydrogen and control plasmas, the power supply and Evenson cavity tuning were adjusted such that the forward and reflected powers indicated by the power reading diodes (Agilent) of the Opthos generator were identical.

In general, the ultimate basis of any microwave power measurement is a direct absolute calorimetric determination on an instrument which then serves as a primary standard for secondary measurements. In our experiments, that absolute standard was the water bath calorimeter at fixed forward and reflected power diode settings. For example, with the assumption that krypton plasma does not produce excess heat, the power

dissipated in the load is absolutely known at particular fixed forward and reflected power diode readings from the calorimetric measurement. Thus, if the diode values are matched identically for any other plasma load, the power dissipated in that load must be identical since the system and the measured power flows are identical. This was tested by running 40 control plasmas of various pure gases and gas mixtures (e.g. He, Ar, Kr, Kr/H_2, Xe, Xe/H_2, N_2, N_2/H_2, CO_2, CO_2/H_2) with different pressures and mixture ratios [17]. The resulting common water bath reading served as the calibration of the input power to helium–hydrogen plasmas. That is, since presumably the electron density, electron temperature, ionization fraction, hydrogen atom density and energy, and gas temperature are different for all plasmas, if these factors impact the power diode readings, then each different control plasma, even for constant diode readings, would produce a different water bath signal. Thus, the nearly identical heat signals measured for the many control plasmas demonstrate the reliability of the power diodes, set at constant readings, as a means to create identical net power input from the magnetron to each plasma. It should also be noted that each plasma required unique 'stub tuning' to produce the desired forward and reflected power readings. Thus, it is clear that 'tuning' also does not impact the readings of the power diodes.

In addition, a six-turn Ni wire coil antenna was symmetrically wrapped around the outside of the plasma tube, the Evenson cell was centered on the coil, and the power spectrum of the microwave power driving the plasmas was analyzed (Advantest R3265 spectrum analyzer). The power spectrum into all plasmas under the identical operating conditions as the calorimetric studies was determined to be a single peak at 2455 MHz with a full-width at half-maximum of 1 MHz. The relative input power at different diode settings for the forward and reflected power was determined by calibrating the peak height relative to a microwave power meter. The power diodes were determined to respond linearly over a broad range of forward and reflected powers (±20 W) around the particular absolutely calibrated diode readings that were matched in each experiment. Thus, slight mismatches (on the order of ±1 W) were determined to be inconsequential to the results.

Since the cell and water bath system were adiabatic, the general form of the power balance equation with the possibility of excess power is

$$P_{in} + P_{ex} - P_{out} = 0 \quad (7)$$

where P_{in} is the microwave input power, P_{ex} the excess power generated from the hydrogen catalysis reaction, and P_{out} the thermal power loss from the cell to the water bath. The cell typically reached steady state in about 10 min after each experiment was started. At this point, the power lost from the cell P_{out} was equal to the power supplied to the cell, P_{in}, plus any excess power P_{ex}.

$$P_{in} + P_{ex} = P_{out} \quad (8)$$

Since the cell was surrounded by water that was contained in an insulated reservoir with negligible thermal losses as discussed above, the temperature response of the thermistor T as a function of time t was modeled by a linear curve

$$\dot{T}(t) = a^{-1} P_{out} \quad (9)$$

where a is the heat capacity (J/°C) for the least square curve fit of the response to power input for the control experiments ($P_{ex} = 0$). The slope was recorded for about 2 h after the cell had reached a thermal steady state, to achieve an accuracy of ±1%.

The slope of the temperature rise as a function of time was recorded for each run and baseline corrected for the negligible stirrer power and loss to ambient, then the output power was calculated from the corrected slope. After the calorimeter was calibrated, $T(t)$ was recorded with a selected setting of the forward and reflected power to the control plasma. The slope was determined with this constant forward and reflected microwave power, and the microwave input power was absolutely determined for these panel meter readings using Eq. (9) with the $\dot{T}(t)$ response and the heat capacity a. Then, identical forward and reflected microwave power settings were replicated for the helium–hydrogen mixture and $T(t)$ was again recorded. The higher slope produced with helium–hydrogen mixture, having He^+ as a catalyst and atomic hydrogen as a reactant, compared with controls with no hydrogen and no catalyst present was representative of the excess power. In the case of the catalysis run, the total output power P_{out} was determined by solving Eq. (9) using the measured $\dot{T}(t)$ and the heat capacity a. The excess power P_{ex} was determined from Eq. (8).

3. Results and discussion

3.1. EUV spectroscopy

In the case of the EUV spectrum of hydrogen, xenon, or xenon–hydrogen (98/2%), no peaks were observed below 78 nm, and no spurious peaks or artifacts due to the grating or the spectrometer were observed. Only known He I and He II peaks were observed in the EUV spectrum of the control helium microwave discharge cell emission.

The EUV spectra (17.5–50 nm) of the microwave cell emission of the helium–hydrogen mixture (98/2%) (top curve) and the helium control (bottom curve) are shown in Fig. 4. Ordinary hydrogen has no emission in these regions. Novel peaks were observed at 45.6, 37.4, and 20.5 nm which do not correspond to helium. At the 1 Torr condition, additional novel peaks were observed in the short wavelength region (5–50 nm) at 14.15, 13.03, 10.13, and 8.29 nm which do not correspond to helium as shown in Fig. 4. Known He I lines which were used for calibration of the novel peak positions were observed at 58.4, 53.7, and 52.4 nm. It is proposed that the 30.4 nm peak shown in Figs. 4 and 5 was not entirely due to the He II transition. In the case of the helium–hydrogen mixture, the ratio of 30.4 nm (40.8 eV) peak to the 25.6 nm (48.3 eV) peak was 10 compared to 5.4 for helium alone as shown in Fig. 4 which implies only a minor He II transition contribution to the 30.4 nm peak.

It is proposed that the majority of the 91.2 nm peak was also due to a novel transition. At 20 Torr, the ratio of the Lyman β peak to the 91.2 nm peak of the helium–hydrogen plasma was two compared to eight for each control hydrogen and xenon–hydrogen plasma which indicates that the majority of the

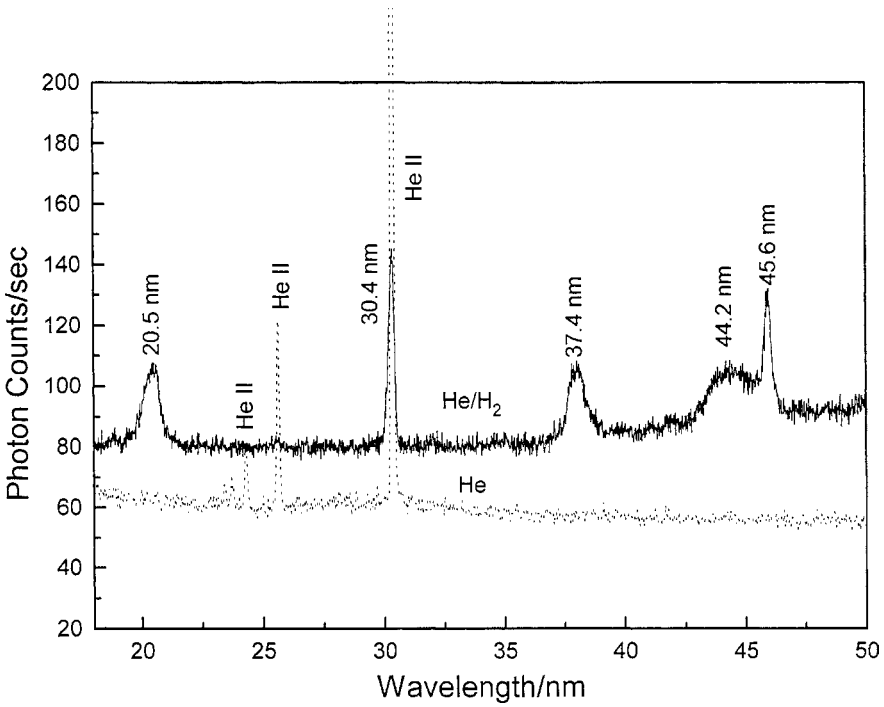

Fig. 4. The EUV spectra (17.5–50 nm) of the microwave cell emission of the helium–hydrogen mixture (98/2%) (top curve) recorded at 20 Torr with a normal incidence EUV spectrometer and a CEM, and control helium (bottom curve) recorded at 20 Torr with a 4° grazing incidence EUV spectrometer and a CEM. Only known He I and He II peaks were observed with the helium control. Reproducible novel emission lines were observed at 45.6 and 30.4 nm with energies of $q \times 13.6$ eV, where $q = 2$ or 3 (Eqs. (1) and (3)) and at 37.4 and 20.5 nm with energies of $q \times 13.6$ eV, where $q = 4$ or 6 that were inelastically scattered by helium atoms wherein 21.2 eV was absorbed in the excitation of He ($1s^2$) to He ($1s^1 2p^1$) as proposed in Eq. (15).

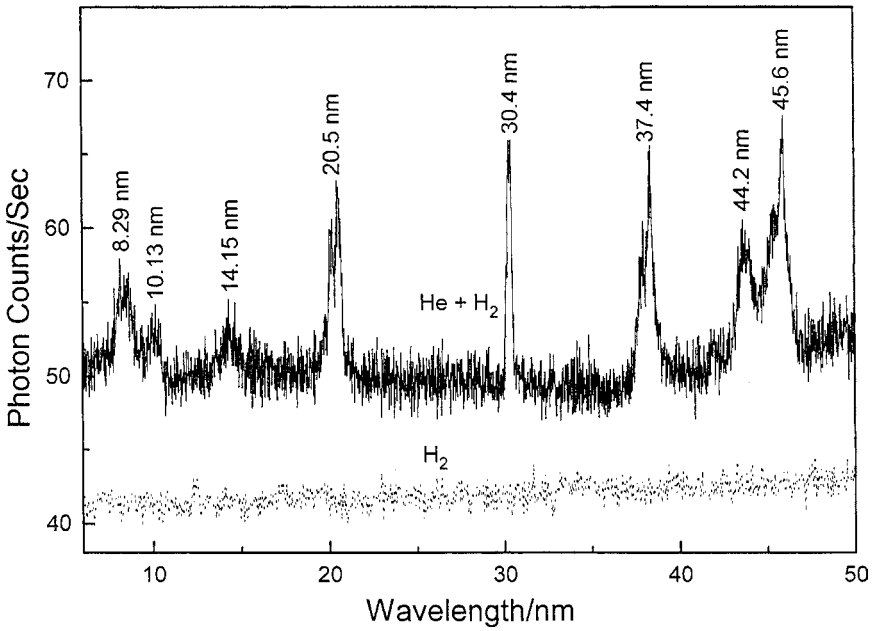

Fig. 5. The short wavelength EUV spectra (5–50 nm) of the microwave cell emission of the helium–hydrogen mixture (98/2%) (top curve) and control hydrogen (bottom curve) recorded at 1 Torr with a normal incidence EUV spectrometer and a CEM. No hydrogen emission was observed in this region, and no instrument artifacts were observed. Reproducible novel emission lines were observed at 45.6, 30.4, 13.03, 10.13, and 8.29 nm with energies of $q \times 13.6$ eV, where $q = 2$, 3, 7, 9, or 11 and at 37.4, 20.5, and 14.15 nm with energies of $q \times 13.6$ eV, where $q = 4$, 6 or 8 that were inelastically scattered by helium atoms wherein 21.2 eV was absorbed in the excitation of He ($1s^2$) to He ($1s^1 2p^1$) as proposed in Eq. (15). The peak at 13.03 nm was observed as a weak shoulder on the 14.15 nm peak, and has been observed in repeated (non-presented) spectra.

91.2 nm peak was due to a transition other than the binding of an electron by a proton.

All known possibilities for the series of novel lines were considered. Known explanations for the novel series of spectral lines and all possible contaminants were ruled out [7]. The only known species in a helium–hydrogen plasma, H^+, H_2^+, H_3^+, H^-, H, H_2, He_2^*, HeH^+, and remotely possible HeH were eliminated since the spectra did not match or the species could not exist under the reaction conditions. Other exotic possibilities such as He_2^+, HHe_2^+, HHe_n^+ and He_n were eliminated due to the extremely specialized conditions required for their formation such as extremely low temperatures that were unlike those in the helium–hydrogen microwave plasmas [32,33]. Air contaminants were also eliminated. Plasmas of nitrogen, oxygen, carbon dioxide, or these gases with 2% hydrogen showed no emission in the region <50 nm for hydrogen mixed with nitrogen, oxygen, and carbon dioxide. In addition, water vapor present in the oxygen–hydrogen plasma showed no emission in this region. Emission of argon, krypton, and xenon as helium contaminants were eliminated. No emission was observed in the region <50 nm for xenon, xenon–hydrogen, krypton, and krypton–hydrogen, and argon and neon were eliminated based on spectral line mismatches and absences. Silicon from the quartz tube wall was eliminated since emission due to Si I, Si II, or Si III is not possible below 56 nm based on the NIST tables [34]. No pump contaminants were possible.

The novel peaks fit two empirical relationships. In order of energy, the set comprising the peaks at 91.2, 45.6, 30.4, 13.03, 10.13, and 8.29 nm correspond to energies of $q \times 13.6$ eV, where $q = 1$, 2, 3, 7, 9, 11. In order of energy, the set comprising the peaks at 37.4, 20.5, and 14.15 nm correspond to energies of $q \times 13.6$–21.21 eV, where $q = 4$, 6, 8. These lines can be explained as electronic transitions to fractional Rydberg states of atomic hydrogen given by Eqs. (1)

and (3) wherein the catalytic system involves helium ions because the second ionization energy of helium is 54.417 eV, which is equivalent to 2×27.2 eV. In this case, 54.417 eV is transferred nonradiatively from atomic hydrogen to He^+ which is resonantly ionized. The electron decays to the $n = 1/3$ state with the further release of 54.417 eV which may be emitted as a photon. The catalysis reaction is

$$54.417\,\text{eV} + He^+ + H[a_H] \rightarrow He^{2+} + e^- + H\left[\frac{a_H}{3}\right] + 108.8\,\text{eV} \quad (10)$$

$$He^{2+} + e^- \rightarrow He^+ + 54.417\,\text{eV} \quad (11)$$

And, the overall reaction is

$$H[a_H] \rightarrow H\left[\frac{a_H}{3}\right] \rightarrow 54.4\,\text{eV} + 54.4\,\text{eV} \quad (12)$$

Since the products of the catalysis reaction have binding energies of $m \times 27.2$ eV, they may further serve as catalysts. Thus, further catalytic transitions may occur

$$n = \tfrac{1}{3} \rightarrow \tfrac{1}{4}, \quad \tfrac{1}{4} \rightarrow \tfrac{1}{5},$$

and so on.

Electronic transitions to Rydberg states given by Eqs. (1) and (3) catalyzed by the resonant nonradiative transfer of $m \times 27.2$ eV would give rise to a series of emission lines of energies $q \times 13.6$ eV, where q is an integer. It is further proposed that the photons that arise from hydrogen transitions may undergo inelastic helium scattering. That is, the catalytic reaction

$$H[a_H] \overset{He^+}{\rightarrow} H\left[\frac{a_H}{3}\right] + 54.4\,\text{eV} + 54.4\,\text{eV} \quad (13)$$

yields 54.4 eV by Eq. (11) and a photon of 54.4 eV (22.8 nm). Once emitted, the photon may be absorbed or scattered. When this photon strikes He ($1s^2$), 21.2 eV may be absorbed in the excitation to He ($1s^1 2p^1$). This leaves a 33.19 eV (37.4 nm) photon peak and a 21.2 eV (58.4 nm) photon from He ($1s^1 2p^1$). Thus, for helium the inelastic scattered peak of 54.4 eV photons from Eq. (10) is given by

$$E = 54.4\,\text{eV} - 21.21\,\text{eV} = 33.19\,\text{eV}\,(37.4\,\text{nm}) \quad (14)$$

A novel peak shown in Figs. 4 and 5 was observed at 37.4 nm. Furthermore, the intensity of the 58.4 nm peak corresponding to the spectra shown in Fig. 4 was about 60,000 photons/s. Thus, the transition He ($1s^2$) → He ($1s^1 2p^1$) dominated the inelastic scattering of EUV peaks. The general reaction is

$$\text{photon}\,(h\nu) + \text{He}\,(1s^2) \rightarrow \text{He}\,(1s^1 2p^1) + \text{photon}\,(h\nu - 21.21\,\text{eV}) \quad (15)$$

The two empirical series may be combined—one directly from Eqs. (1) and (3) and the other indirectly with Eq. (15). The energies for the novel lines in order of energy are 13.6, 27.2, 40.8, 54.4, 81.6, 95.2, 108.8, 122.4 and 149.6 eV. The corresponding peaks are 91.2, 45.6, 30.4, 37.4, 20.5, 13.03, 14.15, 10.13, and 8.29 nm, respectively. Thus, the identified novel lines correspond to energies of $q \times 13.6$ eV, where $q = 1, 2, 3, 4, 6, 7, 8, 9, 11$ or these lines inelastically scattered by helium atoms wherein 21.2 eV was absorbed in the excitation of He ($1s^2$) to He ($1s^1 2p^1$). The values of q observed are consistent with those excepted based on Eq. (12) and the subsequent autocatalyzed reactions as discussed previously [6]. The satellite peak at 44.2 nm shown in Figs. 4 and 5 may be due to excimer emission with multipole coupling as discussed elsewhere [7]. The broad line width of the H ($1/p$) lines is consistent with the mechanism involving a nonradiative energy transfer to a species that satisfies the catalyst criterion—a chemical or physical process with an enthalpy change equal to an integer multiple of 27.2 eV. The observation in Fig. 4 that the 30.4 nm is broader than that of the control further supports the assignment to fractional Rydberg state hydrogen. There is remarkable agreement between the data and the proposed transitions to fractional Rydberg states and these lines inelastically scattered by helium according to Eq. (15). All other peaks could be assigned to He I, He II, second order lines, or atomic or molecular hydrogen emission. No known lines of helium or hydrogen explain the $q \times 13.6$ eV related set of peaks.

3.2. Line broadening and T_e measurements

The Doppler-broadened line shape for atomic hydrogen has been studied on many sources such as hollow cathode [35,36] and rf [37,38] discharges. The method of Mills et al. and Videnovic et al. [14,35] was used to calculate the energetic hydrogen atom densities and energies from the intensities and widths of the 656.3 nm Balmer α lines. The 656.3 nm

Balmer α line width recorded with a high resolution (±0.006 nm) visible spectrometer on microwave discharge plasmas of hydrogen compared with each of xenon–hydrogen (90/10%) and helium–hydrogen (90/10%) are shown in Figs. 6 and 7, respectively. The average helium–hydrogen Doppler half-width was not appreciably changed with pressure. The corresponding energy of 180–210 eV and the number density of $5 \times 10^{14} \pm 20\%$ atoms/cm^3, depending on the pressure, were significant compared to only ≈3 eV and 7×10^{13} atoms/cm^3 for pure hydrogen, even though 10 times more hydrogen was present. Only ≈3 eV broadening was observed with control xenon–hydrogen (90/10%) ruling out collisional broadening. The xenon–hydrogen plasma number density of 3×10^{13} atoms/cm^3 was much lower than that of the helium–hydrogen plasma. Furthermore, only the hydrogen lines of the helium–hydrogen plasma, were broadened. The addition of hydrogen to helium had no effect on the helium lines as shown for the 667.816 nm He I line in Fig. 8.

Similarly, the average electron temperature for helium–hydrogen plasma was 30,500 ± 5% K. Whereas, the corresponding temperature of helium alone was only 7400 ± 5% K, and hydrogen alone was 6700 ± 5% K. No high electric field was present in our experiments (e.g. >1 kV/cm in glow discharge plasmas).

We have assumed that Doppler broadening due to thermal motion was the dominant source to the extent that other sources may be neglected. This assumption was confirmed when each source was considered. In general, the experimental profile is a convolution of a Doppler profile, an instrumental profile, the natural (lifetime) profile, Stark profiles, van der Waals profiles, a resonance profile, and fine structure. The contribution from each source was determined to be below the limit of detection [13,14].

Furthermore, no hydrogen species, H^+, H_2^+, H_3^+, H^-, H, or H_2, responds to the microwave field; rather, only the electrons respond. But, the measured electron temperature was about 1 eV; whereas, the measured H temperature was 180–210 eV. This requires that $T_H \ggg T_e$. This result cannot be explained by electron or external Stark broadening or electric field acceleration of charged species. The electron density

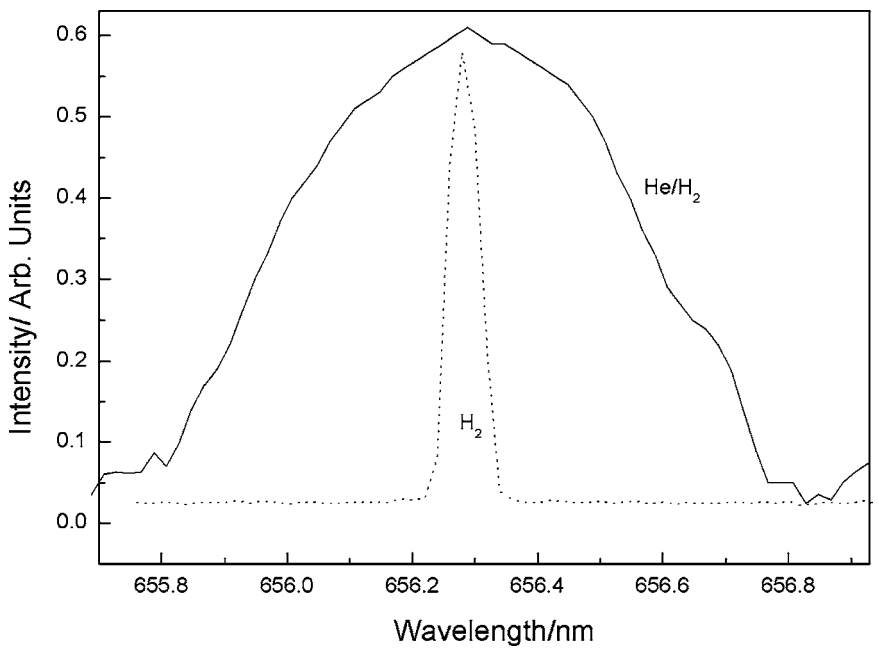

Fig. 6. The 656.3 nm Balmer α line width recorded with a high resolution (±0.006 nm) visible spectrometer on a xenon–hydrogen (90/10%) and a hydrogen microwave discharge plasma. No line excessive broadening was observed corresponding to an average hydrogen atom temperature of 3–4 eV.

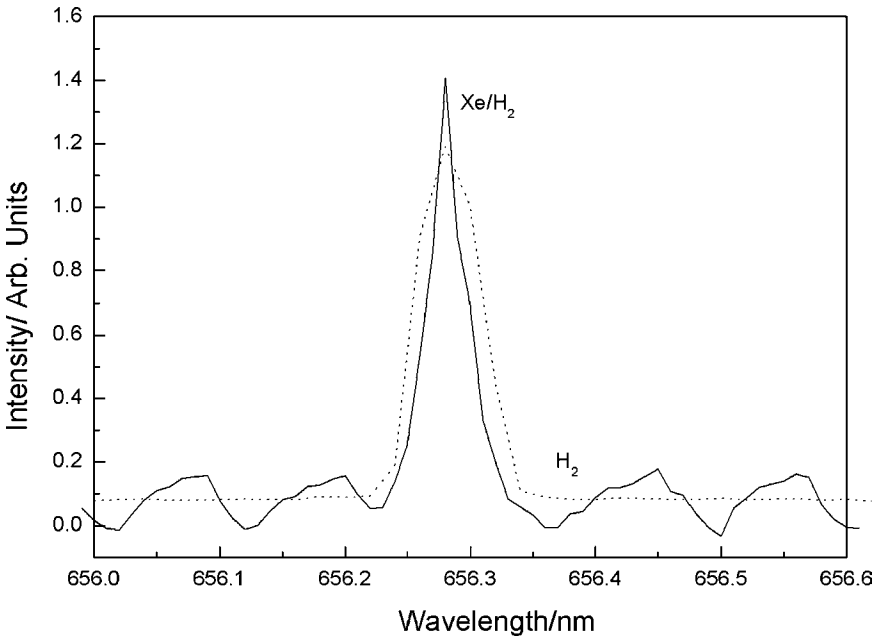

Fig. 7. The 656.3 nm Balmer α line width recorded with a high resolution (±0.006 nm) visible spectrometer on a helium–hydrogen (90/10%) and a hydrogen microwave discharge plasma. Significant broadening was observed corresponding to an average hydrogen atom temperature of 180–210 eV.

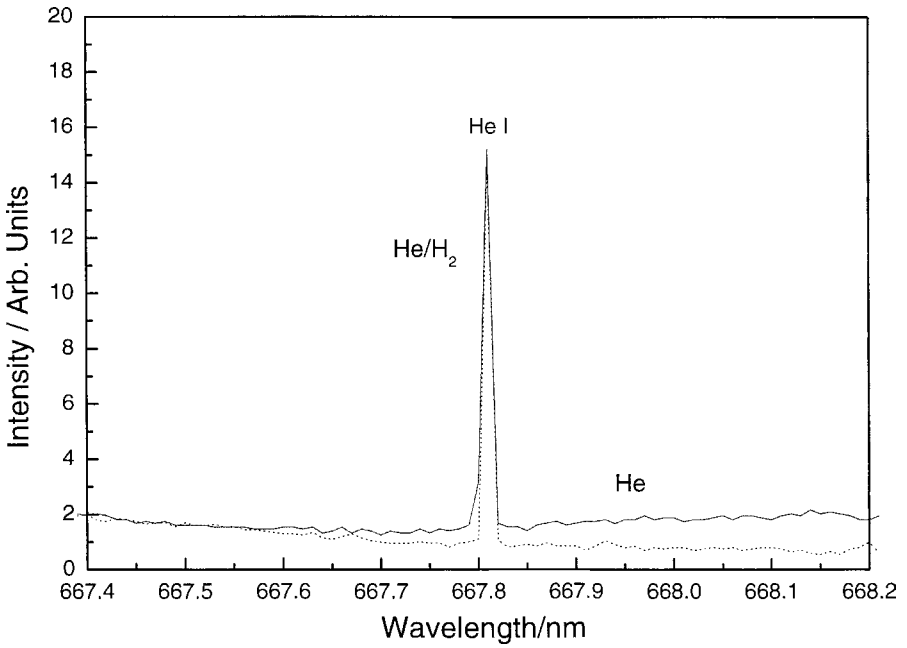

Fig. 8. The 667.816 nm He I line width recorded with a high resolution (±0.006 nm) visible spectrometer on helium–hydrogen (90/10%) and helium microwave discharge plasmas. No broadening was observed in either case.

was five orders of magnitude too low [13,14]. And, in microwave driven plasmas, there is no high electric field in a cathode fall region (>1 kV/cm) to accelerate positive ions as proposed previously [35–38] to explain significant broadening in hydrogen containing plasmas driven at high voltage electrodes. It is impossible for H or any H-containing ion which may give rise to H to have a higher temperature than the electrons in a microwave plasma. The observation of excessive Balmer line broadening in a microwave driven plasma requires a source of energy other than that provided by the electric field. We propose that the source is the hydrogen catalysis reaction given by Eqs. (10)–(12) followed by subsequent reactions to further lower-energy states given by Eqs. (1) and (3).

The formation of fast H can be explained by a resonant energy transfer from hydrogen atoms to He^+ ions of two times the potential energy of atomic hydrogen, 2×27.2 eV, followed by a collisional energy transfer to yield fast H ($n = 1$) as well as the emission of $q \times 13.6$ eV photons discussed in Section 3.1. For example, the exothermic chemical reaction of H + H to form H_2 does not occur with the emission of a photon. Rather, the reaction requires a collision with a third body, M, to remove the bond energy—$H + H + M \rightarrow H_2 + M^*$ [25]. The third body distributes the energy from the exothermic reaction, and the end result is the H_2 molecule and an increase in the temperature of the system. In the case of the catalytic reaction (Eqs. (10)–(12)) with the formation of states given by Eqs. (1) and (3), the temperature of H becomes very high.

3.3. Helium–hydrogen glow discharge emission spectrum

It was reported previously [13] that a substantial increase in the Lyman and Balmer line emission intensities was observed with the addition of 5% argon to a hydrogen microwave discharge plasma wherein Ar^+ served as the catalyst. The EUV spectra (90–130 nm) and (400–520 nm) of the cell emission from the hydrogen glow discharge plasma (dotted line) and the hydrogen glow discharge plasma to which 5% helium was added (solid line) are shown in Figs. 9 and 10, respectively. Upon the addition of 5% helium, the hydrogen Lyman and Balmer line emission intensities approximately doubled which is indicative of a more energetic plasma. However, the catalysis rate was not sufficiently high enough to produce detectable emission of the novel series of lines observed with the Evenson microwave cell. We had shown previously that the conditions of the particular discharge may be a major parameter in the observation of excessive Doppler Balmer line broadening with plasmas of hydrogen and a noble ion having an ionization potential of an integer multiple of 27.2 eV [2–5,7,12–14,18,19] as well as population inversion with oxygen as the catalyst [18,19]. We proposed that the Evenson microwave cavity with appropriate tuning discussed in Section 3.4 provides favorable conditions for the catalytic reaction of He^+ with atomic hydrogen.

3.4. Comparison of the intensity of He I and He II peaks with the addition of hydrogen to a helium microwave plasma

The results of the addition of 5% hydrogen to a helium microwave plasma maintained in the Evenson cavity with a forward power of 100 W and a reflected power of 30 W is shown in Fig. 11. The broad peaks with a separation of 1.18 eV in the 27–65 nm region that were observed with the addition of hydrogen to the helium plasma corresponding to a vibrational series of a molecular ion, H_2 $(1/4)^+$, and were discussed previously [8,9]. Due to the different pressure and flow rate conditions this molecular ion preferably formed and dominated the emission. The He I emission dominated for pure helium; whereas, He II emission dominated with the addition of hydrogen as shown by the comparison of the intensity of the emission of the He II peak at 30.4 nm to that of the He I peak at 58.4 nm. The catalysis reaction of He^+ (Eqs. (10)–(12)) would give rise to increase in He II emission according to the reaction given by Eq. (11); however, the effect of the addition of hydrogen on the intensity of the He II peak before the addition of hydrogen as well as after depended on the tuning of the cavity. The microwave electric field of the Evenson cavity can be increased with appropriate tuning [30,31]. This condition corresponded to a high forward as well as a high reflected power. The intensity of the $q \times 13.6$ eV related set of peaks, the Balmer line broadening, the elevated T_e, and the excess power measured on helium–hydrogen microwave plasmas given in Sections 3.1, 3.2 and 3.5, respectively, showed the same dependency.

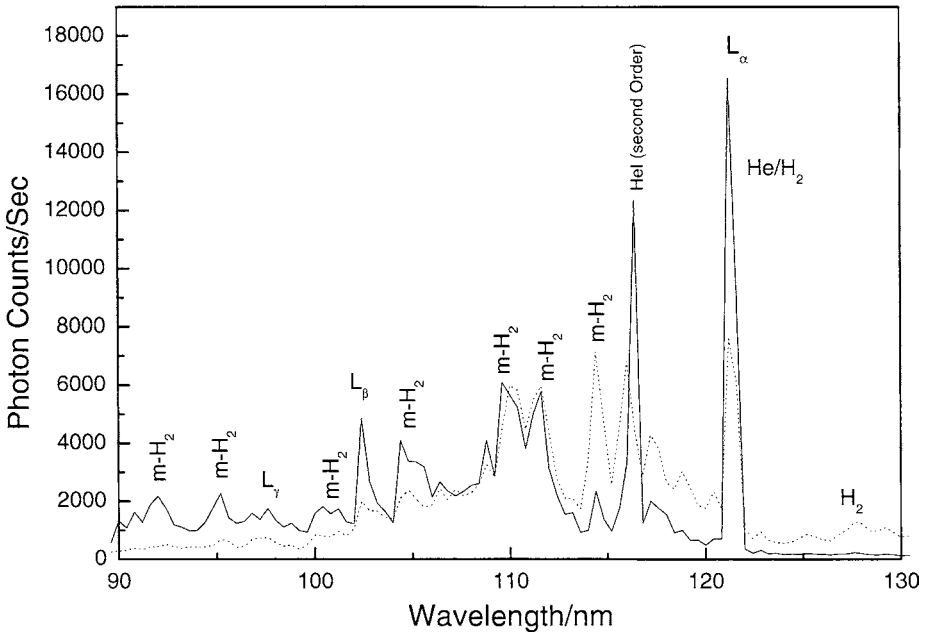

Fig. 9. The EUV spectra (90–130 nm) of the glow discharge light source emission from the hydrogen plasma (dotted line) and the hydrogen plasma to which 5% helium was added (solid line) which shows the increase in hydrogen L_α emission.

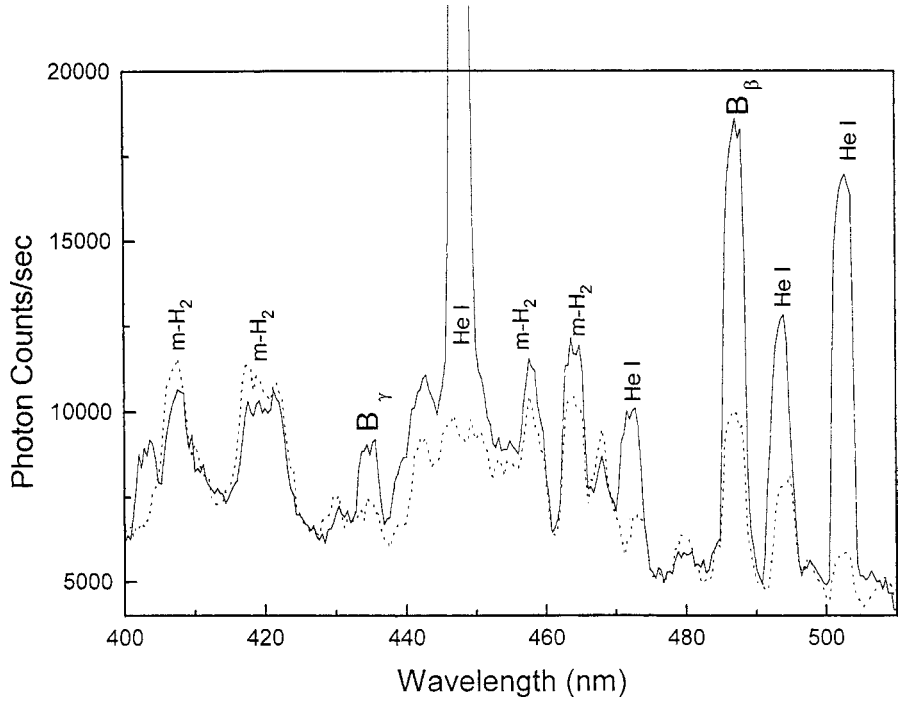

Fig. 10. The EUV spectra (400–520 nm) of the glow discharge light source emission from the hydrogen plasma (dotted line) and the hydrogen plasma to which 5% helium was added (solid line) which shows the increase in hydrogen B_β and B_γ emission.

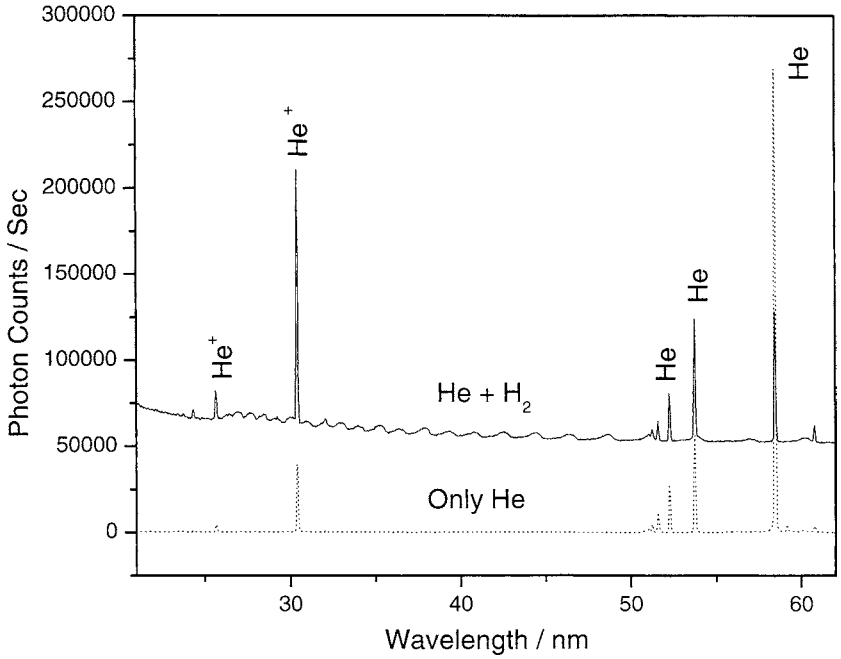

Fig. 11. The EUV spectra (20–60 nm) of the microwave cell plasma emission of the helium (dotted curve) and the helium–hydrogen mixture (95/5%) (solid curve) recorded at 1 Torr with a 4° grazing incidence EUV spectrometer and a CEM. The plasmas were maintained in the Evenson cavity with a forward power of 100 W and a reflected power of 30 W. The He I emission dominated for pure helium; whereas, He II emission dominated with the addition of hydrogen as shown by the comparison of the intensity of the He II peak at 30.4 nm to that of the He I peak at 58.4 nm.

3.5. Power balance of the hydrogen microwave plasma

The thermogram, $T(t)$ response of the cell, with stirring only and with a constant input power to the high precision heater of 50 W is shown in Fig. 12. The baseline corrected least squares fit of the slope, $\dot{T}(t)$, was 2.622×10^{-4} °C/s, and the heat capacity determined from Eqs. (8) and (9) with $P_{ex} = 0$, and $P_{in} = P_{out} = 50$ W was 1.907×10^5 J/°C. Then the temperature response of the calorimeter for any case (Eq. (9)) was determined to be

$$\dot{T}(t) = (1.907 \times 10^5)^{-1} \times P_{out} \quad (16)$$

The water bath calorimetry is an absolute standard and indicated $P_{in} = 8.1 \pm 1$ W input power at the selected diode settings for all control plasmas. From these results, power input to the helium–hydrogen plasma was confidently known as the diode readings identically matched those of the controls. For example, the $T(t)$ water bath response to stirring and then with selected panel meter readings of the constant forward and reflected microwave input power to krypton was recorded as shown in Fig. 13. Using the corresponding $\dot{T}(t)$ in Eq. (16), the microwave input power was determined to be 8.1 ± 1 W. A helium–hydrogen (90/10%) mixture was run at the same microwave input power readings as the control which corresponded to $P_{in} = 8.1 \pm 1$ W in Eq. (8). The $T(t)$ response was significantly increased for helium–hydrogen (90/10%) as shown in Fig. 13. At 350 min, the pressure was changed from 0.5 to 0.29 Torr. A slight increase in $\dot{T}(t)$ was observed at the lower pressure, possibly due to an increase in atomic hydrogen and He^+. The excess power was determined to be 21.9 ± 1 W from the corresponding $\dot{T}(t)$ using Eq. (16) and (8).

The sources of error were the error in the calibration curve (±0.05 W) and the measured microwave input power (±1 W). The propagated error of the calibration and power measurements was ±1 W.

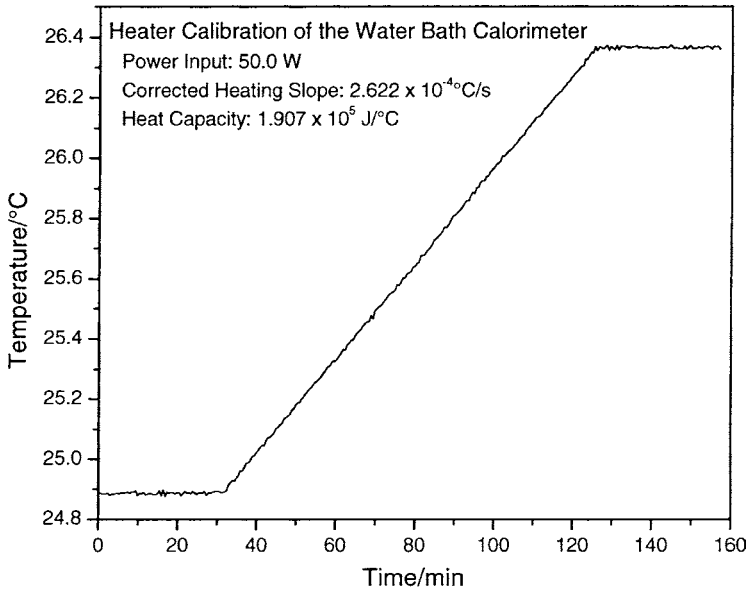

Fig. 12. The thermogram, $T(t)$ response of the cell, with stirring only and with a constant input power to the high precision heater of 50 W. The baseline corrected least squares fit of the slope, $\dot{T}(t)$, was 2.622×10^{-4} °C/s, and the heat capacity was determined to be 1.907×10^5 J/°C.

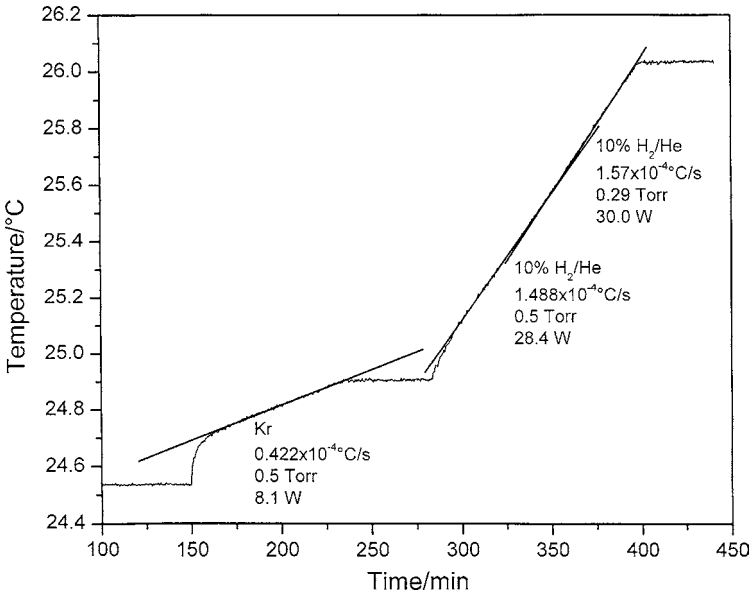

Fig. 13. The $T(t)$ water bath response to stirring and then with selected panel meter readings of the constant forward and reflected microwave input power to krypton was recorded. The microwave input power was determined to be 8.1 ± 1 W. A helium–hydrogen (90/10%) mixture was run at identical microwave input power readings as the control, and the excess power was determined to be 21.9 ± 1 W from the $T(t)$ response.

Given a helium–hydrogen (90/10%) flow rate of 10.0 sccm and an excess power of 21.9 W, energy balances of over -2.9×10^4 kJ/mole H_2 (150 eV/H atom) were measured. The reaction of hydrogen to form water which releases -241.8 kJ/mole H_2 (1.48 eV/H atom) is about 100 times less than that observed. The results indicate that once an atom given by Eqs. (1) and (3) is formed by a catalyst, further catalytic transitions:

$$n = \frac{1}{3} \rightarrow \frac{1}{4}, \quad \frac{1}{4} \rightarrow \frac{1}{5},$$

and so on occur to a substantial extent. This is consistent with the series of lower-energy hydrogen lines with energies of $q \times 13.6$ eV, where $q = 1, 2, 3, 4, 6, 7, 8, 9$, or 11 given in Section 3.1 and elsewhere [4–7], the previously given theory [1–6,22], and previous studies which show very large energy balances [5,7,10,13,17,18].

4. Conclusion

We report that novel emission lines were observed with energies of $q \cdot 13.6$ eV, where $q = 1, 2, 3, 4, 6, 7, 8, 9, 11$ or these lines inelastically scattered by helium wherein 21.2 eV was absorbed in the excitation of He ($1s^2$) to He ($1s^1 2p^1$). These lines were identified as transitions to fractional Rydberg states of atomic hydrogen. An extremely high hydrogen atom temperature of 180–210 eV was observed with the presence of helium ion catalyst only with hydrogen present. Similarly, the average electron temperature for helium–hydrogen plasma was high, $30{,}500 \pm 5\%$ K, compared to $7400 \pm 5\%$ K for helium alone.

The intensity of the emission of the He II peak at 30.4 nm relative to that of the He I peak at 58.4 nm increased with the addition of 5% hydrogen. The effect was dependent on the microwave field which increased the amount of He^+ in both cases. Similarly, hydrogen plasmas became more energetic when helium was added as indicated by the intensification of the Lyman and Balmer emission. The results showed the effect of the presence of He^+ with atomic hydrogen and demonstrated the role of He^+ as a catalyst.

Using water bath calorimetry, excess power was observed from the helium–hydrogen plasma compared to control krypton plasma. For a 8.1 W input, the thermal output power of the helium–hydrogen plasma was measured to be 30.0 W corresponding to 21.9 W of excess power in 3 cm^3. The excess power density and energy balance were high, 7.3 W/cm^3 and -2.9×10^4 kJ/mole H_2, respectively. The results indicate that a new power source based on the catalysis of atomic hydrogen is not only possible, but is it competitive with gas turbine combustion.

The reaction has applications as a new light source, a new field of hydrogen chemistry, and a new source of energy. Since the power is in the form of a plasma, direct high-efficiency, low cost energy conversion may be possible, thus, avoiding a heat engine such as a turbine or a reformer-fuel cell system. Plasmadynamic and photovoltaic power conversion are two promising options [19,39]. Conversion of plasma emission to electricity using a photovoltaic cell irradiation up to 1000 W cm^{-2} (7300 suns equivalent) is currently feasible at high-efficiency [19]. Plasmadynamic conversion of microwave plasma power to electricity has been achieved at about 3.6 W/cm^3 with about 42% efficiency [39]. The lower-energy atomic hydrogen may react to form the corresponding molecule [10]. This nonpollutant product has recently been isolated [40].

Acknowledgements

Special thanks to Y. Lu and T. Onuma for recording some spectra.

References

[1] R. Mills, J. Dong, Y. Lu, Observation of extreme ultraviolet hydrogen emission from incandescently heated hydrogen gas with certain catalysts, Int. J. Hydrogen Energy 25 (2000) 919–943.

[2] R. Mills, M. Nansteel, P. Ray, Argon-hydrogen-strontium discharge light source, IEEE Trans. Plasma Sci. 30 (2) (2002) 639–653.

[3] R. Mills, M. Nansteel, P. Ray, Bright hydrogen-light source due to a resonant energy transfer with strontium and argon ions, New J. Phys. 4 (2002) 70.1–70.28.

[4] R.L. Mills, P. Ray, B. Dhandapani, M. Nansteel, X. Chen, J. He, Spectroscopic identification of transitions of fractional Rydberg states of atomic hydrogen, J. Phys. D, Appl. Phys., submitted for publication.

[5] R.L. Mills, P. Ray, B. Dhandapani, M. Nansteel, X. Chen, J. He, New power source from fractional quantum energy levels of atomic hydrogen that surpasses internal combustion, J. Mol. Struct. 643 (1–3) (2002) 43–54.
[6] R. Mills, P. Ray, Spectral emission of fractional quantum energy levels of atomic hydrogen from a helium-hydrogen plasma and the implications for dark matter, Int. J. Hydrogen Energy 27 (3) 301–322.
[7] R.L. Mills, P. Ray, B. Dhandapani, J. He, Spectroscopic identification of fractional Rydberg states of atomic hydrogen formed by a catalytic helium–hydrogen plasma reaction, AIAA J., submitted for publication.
[8] R. Mills, P. Ray, Vibrational spectral emission of fractional-principal-quantum-energy-level hydrogen molecular ion, Int. J. Hydrogen Energy 27 (5) (2002) 533–564.
[9] R. Mills, J. He, A. Echezuria, B. Dhandapani, P. Ray, Comparison of catalysts and plasma sources of vibrational spectral emission of fractional-Rydberg-state hydrogen molecular ion, Vib. Spectrosc., submitted for publication.
[10] R.L. Mills, P. Ray, J. Dong, M. Nansteel, B. Dhandapani, J. He, Vibrational spectral emission of fractional-principal-quantum-energy-level atomic and molecular hydrogen, Vib. Spectrosc. 31 (2) (2003) 195–213.
[11] R. Mills, P. Ray, Spectroscopic identification of a novel catalytic reaction of potassium and atomic hydrogen and the hydride ion product, Int. J. Hydrogen Energy 27 (2) (2002) 183–192.
[12] R.L. Mills, P. Ray, A comprehensive study of spectra of the bound-free hyperfine levels of novel hydride ion $H^-(1/2)$, hydrogen, nitrogen, and air, Int. J. Hydrogen Energy 28 (8) (2003) 825–871.
[13] R.L. Mills, P. Ray, Substantial changes in the characteristics of a microwave plasma due to combining argon and hydrogen, New J. Phys. 4 (2002) 22.1–22.17, http://www.njp.org.
[14] R.L. Mills, P. Ray, B. Dhandapani, R.M. Mayo, J. He, Comparison of excessive Balmer α line broadening of glow discharge and microwave hydrogen plasmas with certain catalysts, J. Appl. Phys. 92 (12) (2002) 7008–7022.
[15] R. Mills, T. Onuma, Y. Lu, Formation of a hydrogen plasma from an incandescently heated hydrogen-catalyst gas mixture with an anomalous afterglow duration, Int. J. Hydrogen Energy 26 (7) (2001) 749–762.
[16] H. Conrads, R. Mills, Th. Wrubel, Emission in the deep vacuum ultraviolet from a plasma formed by incandescently heating hydrogen gas with trace amounts of potassium carbonate, Plasma Sources Sci. Technol., in press.
[17] J. Phillips, R.L. Mills, X. Chen, Water bath calorimetric study of excess heat in 'resonance transfer' plasmas, J. Appl. Phys., submitted for publication.
[18] A.J. Marchese, P.M. Jansson, J.L. Schmalzel, NASA Institute for Advanced Concepts Phase I Presentation, Atlanta, GA, 25 October 2002, http://www.engineering.eng.rowan.edu/~marchese/finalpres.pdf.
[19] R. Mills, P. Ray, R.M. Mayo, Stationary inverted Balmer and Lyman populations, Highly pumped inverted Balmer and Lyman, submitted for publication.
[20] R. Mills, B. Dhandapani, M. Nansteel, J. He, T. Shannon, A. Echezuria, Synthesis and characterization of novel hydride compounds, Int. J. Hydrogen Energy 26 (4) (2001) 339–367.
[21] R. Mills, B. Dhandapani, N. Greenig, J. He, Synthesis and characterization of potassium Iodo hydride, Int. J. Hydrogen Energy 25 (12) (2000) 1185–1203.
[22] R. Mills, The Grand Unified Theory of Classical Quantum Mechanics, BlackLight Power Inc., Cranbury, New Jersey, September 2001, Distributed by Amazon.com posted at http://www.blacklightpower.com.
[23] R. Mills, The grand unified theory of classical quantum mechanics, Int. J. Hydrogen Energy 27 (5) (2002) 565–590.
[24] R. Mills, The nature of free electrons in superfluid helium—a test of quantum mechanics and a basis to review its foundations and make a comparison to classical theory, Int. J. Hydrogen Energy 26 (10) (2001) 1059–1096.
[25] N.V. Sidgwick, The Chemical Elements and Their Compounds, vol. I, Clarendon Press, Oxford, 1950, p. 17.
[26] M.D. Lamb, Luminescence Spectroscopy, Academic Press, London, 1978, p. 68.
[27] F.F. Chen, Electric probes, in: R.H. Huddleston, S.L. Leonard (Eds.), Plasma Diagnostic Techniques, Academic Press, New York, 1965.
[28] J. Tadic, I. Juranic, G.K. Moortgat, Pressure dependence of the photooxidation of selected carbonyl compounds in air: *n*-butanal and *n*-pentanal, J. Photochem. Photobiol. A: Chem. 143 (2000) 169–179.
[29] R.F. Boivin, J.L. Kline, E.E. Scime, Electron temperature measurement by a helium line ratio method in helicon plasmas, Phys. Plasma 8 (2001) 5303–5314.
[30] F.C. Fehsenfeld, K.M. Evenson, H.P. Broida, Microwave discharges operating at 2450 MHz, Rev. Sci. Instrum. 35 (3) (1965) 294–298.
[31] B. McCarroll, An improved microwave discharge cavity for 2450 MHz, Rev. Sci. Instrum. 41 (1970) 279.
[32] I. Baccarelli, F.A. Gianturco, F. Schneider, Stability and fragmentation of protonated helium dimers from ad initio calculations of their potential energy surfaces, J. Phys. Chem. A 101 (1997) 6054–6062.
[33] J. Higgins, C. Callegari, J. Reho, F. Stienkemeier, W.E. Ernst, M. Gutowski, G. Scoles, Helium cluster isolation spectroscopy of alkali dimers in the triplet manifold, J. Phys. Chem. A 102 (1998) 4952–4965.
[34] NIST Atomic Spectra Database, http://www.physics.nist.gov/cgi-bin/AtData/display.ksh.
[35] I.R. Videnovic, N. Konjevic, M.M. Kuraica, Spectroscopic investigations of a cathode fall region of the Grimm-type glow discharge, Spectrochim. Acta, Part B 51 (1996) 1707–1731.
[36] S. Alexiou, E. Leboucher-Dalimier, Hydrogen Balmer-α in dense plasmas, Phys. Rev. E 60 (3) (1999) 3436–3438.
[37] S. Djurovic, J.R. Roberts, Hydrogen Balmer alpha line shapes for hydrogen-argon mixtures in a low-pressure rf discharge, J. Appl. Phys. 74 (11) (1993) 6558–6565.

[38] S.B. Radovanov, K. Dzierzega, J.R. Roberts, J.K. Olthoff, Time-resolved Balmer-alpha emission from fast hydrogen atoms in low pressure, radio-frequency discharges in hydrogen, Appl. Phys. Lett. 66 (20) (1995) 2637–2639.
[39] R. Mayo, R. Mills, Direct plasmadynamic conversion of plasma thermal power to electricity for microdistributed power applications, in: Proceedings of the 40th Annual Power Sources Conference, Cherry Hill, NJ, 10–13 June 2002, pp. 1–4.
[40] R.L. Mills, B. Dhandapani, M. Nansteel, J. He, P. Ray, Liquid-nitrogen-condensable molecular hydrogen gas isolated from a catalytic plasma reaction, J. Phys. Chem. B, submitted for publication.